

Left Ventricle Computational Model based on Patients Three-dimensional MRI

Maria Narciso¹^a, Ana Isabel Sousa¹^b, Fernando Crivellaro¹^c, Rui Valente de Almeida¹^d,
António Ferreira²^e and Pedro Vieira¹^f

¹*FCT Nova, Caparica, Portugal*

²*Cardiology Department, Hospital de Santa Cruz, Centro Hospitalar Lisboa Ocidental, Lisbon, Portugal*

Keywords: Heart Computational Model, Parallel Simulation, Cardiac Electrophysiology, Arrhythmia, CHASTE, MATLAB, Virtual Heart.

Abstract: The propagation of electric signal in the heart is bonded to the cardiac muscle (myocardium) geometry and condition. In this regard we aim to build a patient-specific computational model of the myocardium based on noninvasive imaging, with the long-term goal of being used to run simulations in electrophysiology studies. Three-dimensional (3D) Magnetic Resonance Images (MRI) were processed using MATLAB[®] to build a volumetric mesh which embodies the Left Ventricle (LV) and can later be read by third party applications. This feature was tested with the open source software CHASTE (Cancer, Heart and Soft Tissue Environment) to solve and visualize the propagation of an excitation wave.

Furthermore, an algorithm was developed capable of defining the fibre orientation for the resulting mesh, based on the geometry described in literature. This experiment substantiates the expectation that parallel computing simulations of the heart maybe used, in the near future, as a monitoring and diagnostic tool for the assessment of cardiac arrhythmias in clinical practice.

1 INTRODUCTION

The work here described is part of a project currently being developed in collaboration with Hospital de Santa Cruz (Carnaxide, Portugal), where Physicians and Techs contribute with not only datasets but, above all, guidance and expertise. The ultimate goal is to create an arrhythmia risk-stratification tool using noninvasive imaging as input. In order to accomplish this, it is fundamental to develop a method capable of assembling a 3D model of the heart, more specifically of the LV, from the imaging datasets. This paper will be focused on this very first step of the process.

Cardiac electric impulses begin at the sinoatrial node (natural pacemaker) and spread through the myocytes, cardiac cells with membranes selectively permeable to K, Na and Ca ions. The movement of these

ions in and out of the intracellular space causes the potential difference responsible for driving the electrical signals to the contractile myocytes (Tse, 2016)(Di Yu et al., 2014).

The heart walls that enclose the four cardiac chambers are formed by myocardium, the muscular tissue responsible for the heart contraction. The inner part of the myocardium is called endocardium, while the outermost part is usually called epicardium. Most of the ventricular arrhythmias are the result of some form of structural heart disease that causes the myocardial tissue to become heterogeneous in terms of electric conduction. Since most of the clinically significant ventricular arrhythmias arise from the LV, and in order to simplify the model and reduce computational costs, we limited our analysis to this ventricle.

Cardiac magnetic resonance has started to replace ultrasound-based echocardiograms as the imaging standard in clinical arrhythmology and electrophysiology studies (De Maria et al., 2017). Beside the advantage of being non-invasive while not using ionizing radiation. MRI provides excellent contrast between soft tissues, offering structural and functional information. The images are computational re-

^a <https://orcid.org/0000-0001-5079-9381>

^b <https://orcid.org/0000-0003-2980-4742>

^c <https://orcid.org/0000-0002-7534-9149>

^d <https://orcid.org/0000-0002-2269-7094>

^e <https://orcid.org/0000-0002-1623-7382>

^f <https://orcid.org/0000-0002-3823-1184>

constructions of the signal received from sensors that measure the particles resonance when cut off from an excitation pulse of radio waves. Although this technology alone is not capable of detecting fibres and micro structures, the anatomical features extracted from the resulting images provide the most advantageous baseline to achieve *in silico* patient-specific heart models. (Auricchio, Angelo, Singh, Jagmeet, Rademakers, 2012). For this reason, this was the imaging modality chosen as outset of our project.

Technical details of the method that has proven to be able to generate three-dimensional models from these images are described in the next chapter. Image processing was done in MATLAB and the fibre orientation estimation code was written in Python. The diagram in figure 1 depicts the overall workflow.

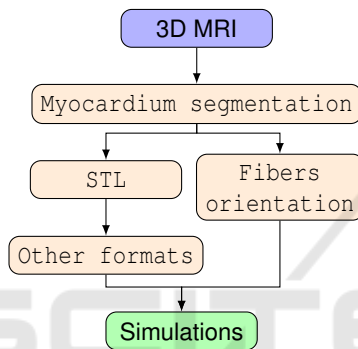


Figure 1: Workflow of the three-dimensional model assembling process.

2 DEVELOPMENT OF THE VENTRICLE MODEL

This section reports the methods used for developing the 3D computational model of the LV, built from magnetic resonance images of a specific patient. The methods described were designed in MATLAB 2015 and trusted to be broad enough to be used with most patients, aside from subjects with severe cardiac deformities, as these cases are not standardized and would require specially designed tools. The result is a Stereolithography (STL) file representing the cardiac muscle, which may later be opened and modified by several applications.

2.1 Dataset

António Ferreira provided anonymized images in DICOM format from a contrast-enhanced 3D cardiac MRI exam that was considered to be entirely normal. Any areas of myocardial fibrosis would be visible in the images as brighter areas amidst the darker cardiac

muscle. Therefore our process started from an ideal case with homogeneous myocardial tissue.

The encoded images are made of voxels, the basic element of a 3D image, in the same manner the pixel is in 2D images. A voxel has three dimensions therefore it is referenced in space by three coordinates, its intensity value can be in several different ranges as the scales are not standardized.

In this acquisition, the whole slab is encoded resulting in 3D image with high spatial resolution - size of an individual voxel - and high signal-to-noise ratio. The voxels are nearly isotropic, allowing reconstruction in any direction.

2.2 Segmentation of MR Data Set

From now on, the first dimension elements of any 3D matrix will be referred to as rows (along yy), the second columns (along xx) and the third slices (along zz).

Information as voxel size, number of rows and columns of each image, was obtained from the DICOM file *info* section and stored with the purpose of being accessed along the process. The images, which represent axial slices of the torso, were read to a three-dimensional matrix with the dimensions *rows* x *columns* x *number of images*, meaning they were turned into two dimensional matrices stacked along the z axis. The intensity values of every image are divided by the maximum value of intensity, to obtain a range from 0(lightest) to 1 (darkest), therefore the rest of the transformations can be applied in any set independently of the scale used in the exam, as of today there is still not a standard range.

Our aim was not to develop an algorithm capable of automatically segment the myocardium but to develop semi-automatic tools to do so, as in this context it was required that a physician guided and supervised the entire process.

The first required transformation is the rotation of the matrix in order to attain the short-axis (SAX) view. In this view, slices are perpendicular to the long-axis (LAX) of the LV which allows us to examine cross-sections of both ventricles, where the chambers walls are clearly distinguishable and the left ventricle sections are usually annular.

Heart orientation and consequently the left ventricle alignment, differs between individuals. On this account and following the traditional cardiologist approach, we chose to navigate through the different perspectives using cutting planes, illustrated by lines the user defines.

As the licensed version of Matlab we had available did not support the *imrotate3d* function - which allows the rotation of three dimensional objects in any

direction at any angle - we defined a function which rotates each slice (two dimensional rotation) around its centre, the same number of degrees the drawn line makes with the vertical axis. Next the whole matrix is rotated 90° clockwise around the y axis, as the function *rot90* is available in this version of the software and allows the use of angles multiples of 90° . The logic of the cutting plan is exemplified in figure 2.

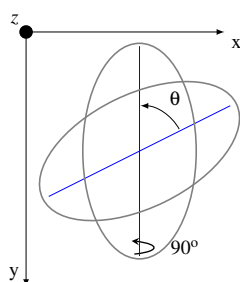


Figure 2: Rotation of 2D images based on the drawn lines, first in the amplitude of θ around the z axis and then 90° around the y axis.

For each transformation triggered by a line, two new matrices are created, first a copy of the original, with the same size but with each slice rotated and cropped, and with the second transformation another copy with the first and third dimensions permuted.

Starting from the axial view, the first line must be parallel to the inter-ventricular septum, right picture of figure 3, the rotation results in the vertical long axis view shown in the left picture of 3. Then one should draw a bisecting line from the LV apex to the mitral valve, this leads to the horizontal long axis view. The user is then asked to mark the LV ventricle apex with a point and the base with a line, figure 4, finally we are presented with the SAX view. This cut generates a matrix with the dimensions *number of rows of each image x columns x number of slices from base to apex*. An example of a slice from this object is shown in figure 5.

Inside the LV chamber, the pixels represent blood therefore the intensity levels are lower than that at the pixels representing tissue. A point in this area and another one at the myocardium outside border are manually marked.

The *grayconnected* function is applied to select the contiguous regions with similar intensities for both points. The output is a binary image where the pixels that are part of the region have the value *one*. The two resulting areas enclose every pixel with values between *seedvalue-tolerance* and *seedvalue+tolerance*. For the area inside the chamber seedvalue is the pixel intensity level at the selected point and the tolerance is a quarter of the difference between this value and the intensity value at the sec-

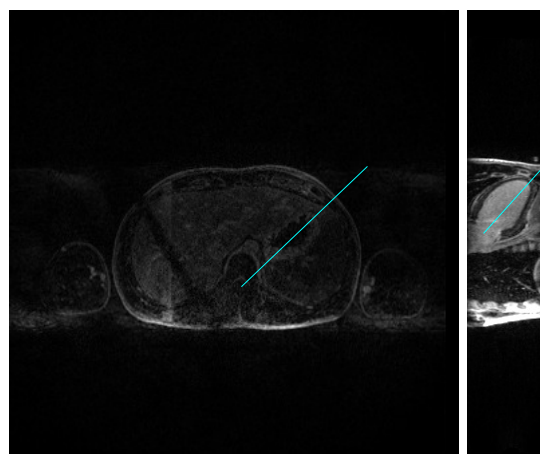


Figure 3: Right: Axial view of the torso with a line drawn parallel to the septum. Left: LAX vertical view with the bisectrix line.

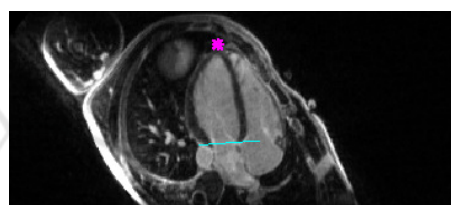


Figure 4: Horizontal LAX view with the apex marked in pink and base of LV in cyan.

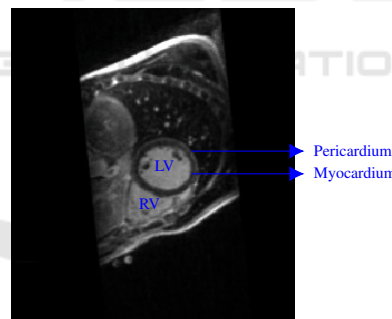


Figure 5: SAX view where both ventricles are visible.

ond point, hence adding only pixels with values closer to the blood intensity than to the muscle. The shape centre of mass is calculated and stored. The second region is the actual segmented myocardium, generated following the same logic. There is a thin protective layer surrounding the whole heart named pericardium, figure 5. Because it is almost white, its pixels are beyond the intensity threshold and will not be aggregated, however this layer is so thin that sometimes its borders are not distinguishable, therefore the distance between the centre of mass is set as the maximum distance the value of the pixels above this radius are change to zero. The result is a black and white im-

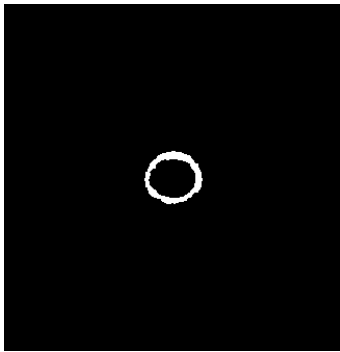


Figure 6: Binary image of the LV myocardium segmented from the SAX slice

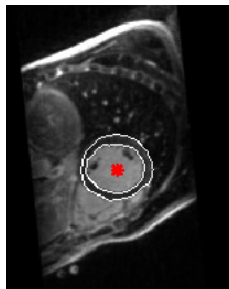


Figure 7: SAX view with the myocardium borders contoured in white and the centre of mass marked with a red cross.

age representing a slice of the myocardium, figure 6, its contours are shown in figure 7 on top of the original slice.

The process above is repeated for every slice, the ones representing the apex myocardium is visible as a small circle, instead of an annulus, therefore only the second point is needed. Each resulting image is saved into a matrix with the same size as the last one created, stacking the cross sections of the ventricle along the third dimension.

2.3 3D Model and Formatting

At this stage the object is represented in a regular grid in 3D space, thus the location of each voxel is described by discrete values of *row*, *column* and *page*, to get the real spacial coordinates the *find* function was called, as it returns the indexes of each voxel with a value not zero and the respective coordinates where saved in a matrix $[r,c,p]$, then each element was multiplied by the voxel size for the respective dimension. This transformation was applied at this stage and not later for the simplicity of working with only point coordinates. Regardless, this is a crucial step considering that, although STL structures are dimensionless and the files contain no scale information, the output must be ready to be handled by applications where

distances and dimensions matter.

It is possible to increase the resolution, multiplying the number of points. Using *linspace* to generate a vector with the size of each dimension, changing the spacing from one to the desired integer number. two *meshgrids* are generated one from the new vectors and one from three vectors with the original spacing. Then using bilinear interpolation with *interp*, a new matrix is created interpolating the original meshgrid with the new one. Higher resolution does not affect the results, however, during the simulations, the signal propagation can be observed with more detail, as the mesh will be made of smaller blocks. As expected, this comes with a high computational price.

The function *alphashape* creates a surface around all the defined points, using the variable alpha to define the tightness, the user defines the optimal alpha value so that the chamber is open while the walls are closed. Next, *boundaryFacets* is called to get the triangles faces and each concerning vertex that form the surfaces of the volume, this process is known as tessellation, filling a surface with geometric shapes (in this case triangles) without overlapping or forming gaps). *smoothpatch* (Kroon, 2010) was applied to polish the rough edges, this function takes each vertex, checks the neighbours from the same facet and moves them in a way that the distance between them becomes more uniform, keeping the number of triangles.

The last step in MATLAB is the exportation to a STL file, supported by many software and applications.

The *stlwrite* (Holcombe, 2011) function was used to export the triangulated structure to a file with the standardized format. Both the smoothed model and the one from the previous step are exported, so they can be tested against each other, ensuring that this aesthetic alterations do not compromise the model. A comparison of both can be found in figure 8.

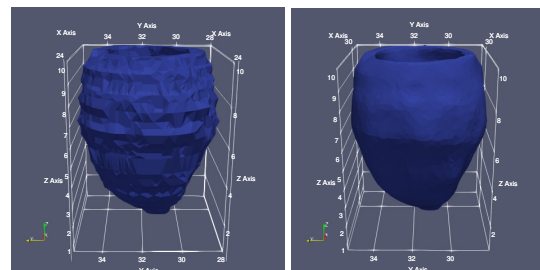


Figure 8: Comparison between the original mesh on the left and the smoothed on the right.

An example of a model build following the methods described, exported with the original resolution and default alpha value, is presented in figure 9.

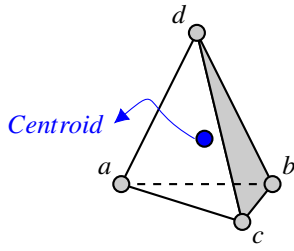


Figure 12: Tetrahedron with nodes a,b,c,d and the calculated centroid.

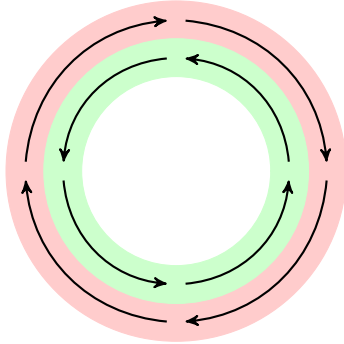


Figure 13: The fibers closer to the outer border of the muscle run.

imagined as a stack of slices as it was during the segmentation. The closer 2D slice value from the registration file to the z coordinate of the centroid will be attributed to this element. All the calculations will be made considering the centroid a point in one of the 2D plans, placed at the annulus.

When the left ventricle contracts to pump the blood it does it by torsion, due to the fact that the muscle fibres run in opposite directions at the inner - endocardium - and outer layers - epicardium - as exemplified in figure 13.

In reality the fibres slope varies according to their distance to the borders, the ones at the endocardium do an angle with the horizontal plan that we will consider approximately -60° and it increases along the muscle till the last layer where we will consider the angle to measure 60° .

Defined by an input variable, a number of circumference radius between the minimum (r_{min}) and maximum (r_{max}) radius is saved in an array, imagining the shape is layered as an onion, the scheme in figure 14 demonstrates a slice divided in six layers and a centroid positioned at the outermost. At the bottom slices of the ventricular apex, the minimum radius is considered zero, figure 15.

Knowing the angle the vector does with the xy plan is a value in $\{-60 : 60\}$, going from the outermost circle to the inner, each radius is matched with an angle θ , according to its position in the ar-

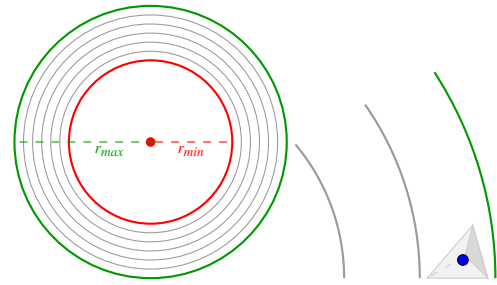


Figure 14: Left: Myocardium split in six layers defined by five radius between r_{min} and r_{max} Right: tetrahedra with centroid at the outermost layer.

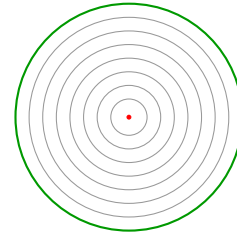


Figure 15: At the apex r_{min} is zero.

ray, which translates in its distance from the centre. The distance between the centroid and the centre is matched with the closer radius from the array, and the θ angle from the orientation vector is therefore assigned. For an element which centroid is located at an inner layer, the angle ϕ the vector does with the x axis is the angle α between the line that connects the centroid with the centre of mass and the vertical line that crosses the centre of mass, plus 90° . As the scheme of figure 16.

For the outer layers, that is when the respective angle θ is positive, the logic is the same, changing only the sum of 90° for a subtraction. Considering the slice of the myocardium a perfect circle, the fibres as in figure 13.

Now returning to the 3D system to calculate the vector third coordinate we know that $\vec{v} = 1$ and both θ and ϕ angles, applying the rules of trigonometry to the scheme in figure 10 the three coordinates of the vector can be calculated by the three equations bellow.

$$x = \cos(\theta) * \cos(\phi) \quad (1)$$

$$y = \cos(\theta) * \sin(\phi) \quad (2)$$

$$z = \sin(\theta) \quad (3)$$

This logic is followed for every element of the mesh, the plot of the the resulting orientation vectors for one of the slices, considering only the 2D plan by setting $z = 0$ is presented in figure 17.

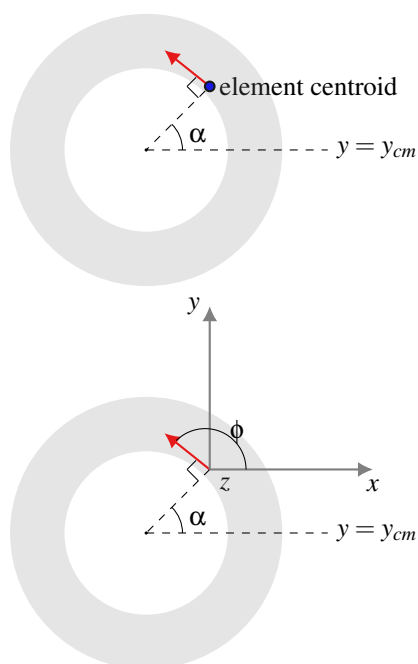


Figure 16: Direction of the vector considering only the xy plan for an element which centroid is located at an inner layer.

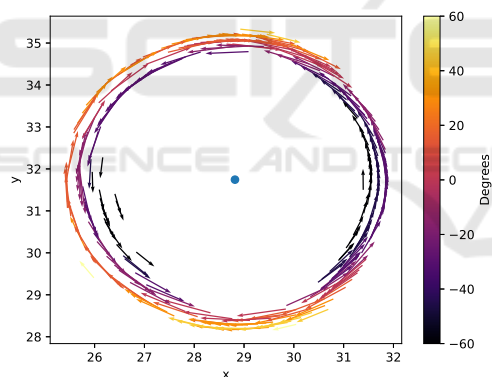


Figure 17: 2D plot of the orientation vectors for one slice, where is visible that that the vectors closer to the centre (blue dot) run anticlockwise and the rest clockwise. From the colormapping its understood that the inner vectors make negative angles with the horizontal xy plan, in 3D, and that this angle gets larger with the proximity to the outer border.

3 RESULTS

To test the model by running electrical simulations, it was decided to work with the open source software CHASTE, developed at Oxford University, as it integrates all the necessary libraries to solve electrical activation problems on biological tissue, offers flexibility and keeps being improved by the community. The cardiac module is capable of recreating the exci-

tation signal propagation throughout adjacent neighbouring cells, using a set of parameters that the user can define (Mirams et al., 2013).

3.1 Simulation

A simulation ran in monodomain, using the Luo-Rudy Backward Euler ionic model and intracellular conductivities of be 3,75 mS/cm for the longitudinal direction and 2.14 mS/cm for transversal and normal. Considering the tissue homogeneous, applying a stimuli of -80.000uA at the apex, pictured in figure 18, after 80 ms the activation spread throughout the ventricle, as shown in figure 19.

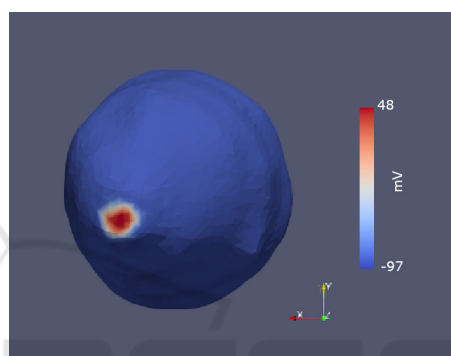


Figure 18: Spherical stimuli at the apex of the smoothed model.

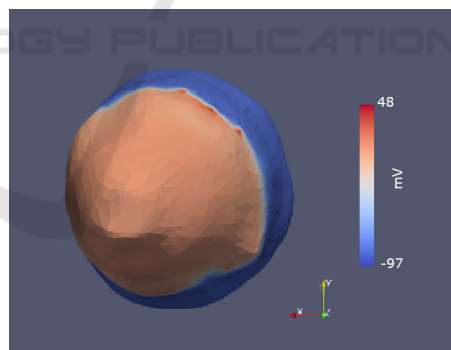


Figure 19: Extension of the activation wave after 90 ms.

4 CONCLUSION

Several research groups have been developing parallel functional models of the heart, however most of the solutions make use of high performance computers. The approach described in this work intends to make use of tools available for free or with student licences. We have proved that it is possible to manipulate the medical images incorporating, in our code, functions available in MATLAB, plus a couple shared

by the community, resulting in an accurate computational model of the LV. These are promising results for the possibility of using non invasive imaging of human cardiac electrical activity for risk assessments in diagnostics.

The next logic step is to map different conductivities accordingly to the intensity levels visible on contrast-enhanced MRI, allowing to perform virtual electrophysiologic studies. In order to accomplish this, the registration process during the segmentation must be replaced by a more accurate method capable of mapping the velocities into a model that must be already a filled volume, unlike the surface one described here.

Open Source C++ Library for Computational Physiology and Biology. *PLoS Computational Biology*, 9(3):e1002970.

Tse, G. (2016). Mechanisms of cardiac arrhythmias. *Journal of Arrhythmia*, 32(2):75–81.

ACKNOWLEDGEMENTS

This work is part of a project co-funded by Fundação para a Ciência e Tecnologia and Compta SA Portugal under the studentship PD/BDE/131399/2017 Ref.CRM:0008003

REFERENCES

- Auricchio, Angelo, Singh, Jagmeet, Rademakers, F. E., editor (2012). *Cardiac Imaging in Electrophysiology*.
- Bayer, J. D., Blake, R. C., Plank, G., and Trayanova, N. A. (2012). A novel rule-based algorithm for assigning myocardial fiber orientation to computational heart models. *Annals of biomedical engineering*, 40(10):2243–54.
- De Maria, E., Aldrovandi, A., Borghi, A., Modonesi, L., and Cappelli, S. (2017). Cardiac magnetic resonance imaging: Which information is useful for the arrhythmologist? *World journal of cardiology*, 9(10):773–786.
- Di Yu, Dongping Du, Hui Yang, and Yicheng Tu (2014). Parallel computing simulation of electrical excitation and conduction in the 3D human heart. In *2014 36th Annual International Conference of the IEEE Engineering in Medicine and Biology Society*, pages 4315–4319. IEEE.
- Holcombe, S. (2011). stlwrite - write ascii or binary stl files. Retrieved May 4, 2018.
- Khaliq, Z. and Pennell, D. (2019). Diffusion tensor cardiovascular magnetic resonance. *Postgraduate medical journal*, 95(1126):433–438.
- Kroon, D.-J. (2010). stlwrite - write ascii or binary stl files. Retrieved March 26, 2010.
- Mirams, G. R., Arthurs, C. J., Bernabeu, M. O., Bordas, R., Cooper, J., Corrias, A., Davit, Y., Dunn, S.-J., Fletcher, A. G., Harvey, D. G., Marsh, M. E., Osborne, J. M., Pathmanathan, P., Pitt-Francis, J., Southern, J., Zenzemi, N., and Gavaghan, D. J. (2013). Chaste: An